Flow, Turbulence and Combustion (2022) 108:819–842
https://doi.org/10.1007/s10494-021-00295-6

Two-Fluid RANS Modelling of Turbulence Created by a Vertically Falling/Moving Particle Cloud

Guodong Gai[1] · Sergey Kudriakov[1] · Olivier Thomine[2] · Stephane Mimouni[3] · Abdellah Hadjadj[4]

Received: 6 August 2020 / Accepted: 25 August 2021 / Published online: 2 September 2021

Abstract
In particle-laden flows, a turbulent field can be produced in the carrier phase by the movement of the particle/spray cloud. In this study, the intensity and the integral length scale of the particle-induced turbulence are studied using a simple mechanistic model with comparison to experimental data and numerical simulations for large-scale numerical applications. The experimental results of DynAsp are investigated with numerical simulation results. Out of the spray nozzle, two regions can be distinguished for the spray dynamics: an inertial zone and an equilibrium zone. It is found that the initial injection velocity of the cloud has little effect on the terminal slip-velocity of the particles in the equilibrium zone far from the injection region. The turbulent kinetic energy is closely related to the particle slip-velocity and shows a maximal value when particles reach their terminal velocity inside the equilibrium zone. The integral length scale depends mainly on three parameters: particle slip-velocity, particle size and volume fraction. Combined with the terminal slip-velocity correlation, the reduced-order mechanistic model can give a reasonable estimation of the turbulent kinetic energy as well as the integral length scale of the particle-laden flow in large-scale configurations.

Keywords Particle cloud · Turbulence modulation · Reduced-order model

1 Introduction

Spray systems can be used as emergency devices in gas processing plants or in offshore platforms. The systems are essential for the prevention of unwanted accidental scenarios, such as hydrogen explosions. In the case of combustion ignition, various regimes

✉ Guodong Gai
guodong.gai@insa-rouen.fr

[1] DEN-DM2S-STMF, CEA, Université Paris-Saclay, 91191 Gif-sur-Yvette, France

[2] CNRS, LIS (UMR 7020), Aix Marseille University, Université de Toulo, Avenue Escadrille Normandie-Niemen, F-13397 Marseille Cedex 20, France

[3] EDF R&D, Fluid Dynamics Power Generation and Environment, 78401 Chatou, France

[4] INSA, CORIA UMR - 6614 CNRS, University of Normand, 76000 Rouen, France

can occur depending on the local concentration of hydrogen, air and water steam, as well as pressure and temperature distributions. In most circumstances, spray devices are installed inside industrial buildings and off-shore platforms, mainly for fire mitigation purposes. A number of experimental investigations have demonstrated that spray systems can have a mitigating effect on flame propagation Wingerden and Wilkins (1995); Thomas (2000). The attenuation relies on the evaporation of small-size water droplets inside the flame Gai et al. (2019). On the contrary, a certain number of experiments Wingerden and Wilkins (1995) resulted in explosion enhancement in the presence of water sprays. It has been established that the main reason for explosion enhancement is the turbulence generated by water sprays in the gas mixture. Depending on the evolution of accident scenarios, ignition might occur before or after the activation of the spray system. Thus, an understanding of the dynamics of water spray in generating turbulence is needed to evaluate its mitigation or enhancement ability during accidental explosions.

Spray- or particle-induced turbulence has been investigated for several decades Hetsroni and Sokolov (1971); Hetsroni (1989); Gore and Crowe (1991); Elghobashi (1994); Sadiki et al. (2005); Xu and Subramaniam (2010); Mallouppas et al. (2017). The presence of particles or a second phase in a continuous flow could change the intrinsic turbulence topology of the carrier flow, which is known as turbulence modulation Crowe et al. (2012). Several key factors arise from various experimental studies that contribute to the turbulence modulation due to the presence of particles Crowe et al. (2012); Gai et al. (2020): surface, inertial, response, loading and interaction effects. Some physical parameters are taken as criteria to distinguish between the attenuation and the enhancement effects of the particle cloud on the carrier flow such as the length scale ratio Gore and Crowe (1989), the particle momentum number *Pa*Tanaka and Eaton (2010), etc.

Several difficulties arise in modelling of phenomenon of turbulence generation by water sprays: *a*) Many factors are involved in the modelling process such as the water flow rate, droplet size, and initial velocity of the droplets. These factors depend on the nozzle type and, in general, are related to each other. Therefore, it is hard to vary each parameter independently. *b*) The industrial sprays have a polydisperse nature. The consequence is that the equilibrium between the gravity and drag forces is reached at different distances from the nozzle, depending on droplet diameter. These distances are short for small-diameter ones, while they could be relatively large for large-diameter droplets. *c*) The nozzles are often placed in linear or circular rows, which leads to an interaction between sprays. This might change not only the droplet size distributions but also the turbulent parameters in the interaction zone.

Ideally, one could imagine an experiment where tracer particles are introduced in the gas affected by the water spray and the turbulence statistics is gathered via, for example Particle Image Velocimetry (PIV) techniques. Unfortunately, to our knowledge, such experimental data are scarcely available in the open literature. Instead, a large amount of experimental data exist on turbulence modulation in the carrier phase by using solid particles. Measurements of air and particle velocities of the two-phase flow in a vertical pipe were made by means of a Laser Doppler Velocimetry (LDV) technique Tsuji et al. (1984). It was noted that the large particles increase the air turbulence throughout the pipe section, while small particles reduce it. In case of turbulence enhancement, the fluctuations were amplified near the pipe centerline and get reduced when approaching the wall Hosokawa and Tomiyama (1998); Hetsroni (1989). Kulick *et al.*Kulick et al. (1994) studied the effects of particles on the fully developed turbulent pipe flow for different particles having smaller sizes compared to the Kolmogorov scale η. The small

particles were found to attenuate the turbulence, with the increase of the Stokes number, the mass loading and the distance from the wall.

A comprehensive research program called DynAsp (Dynamique de l'Aspersion) was carried out in 1996 at CEA in France with aim to build up a series of experiments dealing with exchange of momentum between water spray and ambient gas Patigniez (1996); Herlin et al. (1996). To simplify the problem, the water spray was replaced by solid glass particles. Thus, the deformation, break-up or coalescence of the particles is not taken into account. Laser Doppler Velocimeter (LDV) technique was employed to allow direct measurements of gas velocities in the presence of particles. A standard LDV uses very small particles like tracers to measure the carrier phase movement. Larger dispersed particles produce a stronger signal, which can be discriminated from the carrier phase. For the gaseous carrier phase, the tracers typically have diameters of $\mathcal{O}(1)\ \mu m$, while the dispersed particles have a larger range of diameters of $\mathcal{O}(10-1000)\ \mu m$Balachandar and Eaton (2010). The gas flow velocity was measured by PIV.

Several theoretical and modelling approaches have been developed to understand the turbulence modulation associated with dilute particle-laden flows Yuan and Michaelides (1992); Yarin and Hetsroni (1994); Wacks and Chakraborty (2016); Crowe (2000); Mandø (2009); Mandø et al. (2009). Yuan *et al.* Yuan and Michaelides (1992) developed a simple mechanistic model for turbulence modulation in particle-laden flows based on the interaction of a single particle with turbulent eddies. Kenning *et al.* proposed another simple mechanistic model on turbulence modulation Kenning (1996); Kenning and Crowe (1997). Two sources of turbulent energy of the carrier phase are considered: inherent turbulence of the carrier phase and turbulent energy induced by the relative velocity of the two phases. The turbulent statistics has been presented for mono-dispersed solid particles, which reach terminal velocity inside liquid. For a fully developed dilute particle-laden flow in a vertical pipe, Crowe *et al.* Crowe (2000) simplified the volume averaged turbulent kinetic energy equation by taking into account the turbulence generation via velocity gradients by particle drag and viscous dissipation. However, there is still a lack of a general formulation that can account for most important related factors as stated in Eaton (2006); Saber et al. (2015); Elghobashi (2018).

Given the complexity of the flow, the particle-induced turbulence is difficult to investigate and the direct measurements of the turbulence characteristics are scarcely available in the literature. For the simulations of large-scale configurations in industrial structures, the current existing turbulence models, such as RANS or LES, require an extensive validation and assessment through a series of highly-resolved numerical simulations that are difficult to meet nowadays. These large-scale simulations can be hydrogen explosions in a nuclear confinement building (volume $V = 10^4 \sim 10^5\ m^3$), or offshore facilities (volume $V = 10^5 \sim 10^6\ m^3$) Thomas (2000). The smallest grid sizes for these problems, for practical reasons, cannot be smaller than $\Delta x \approx \mathcal{O}(10\ cm)$, and the direct application of turbulence models such as RANS, involving action of spray and spray-flame interaction, can give erroneous results. The description of spray-induced turbulence in current engineering applications is mostly based on empirical correlations using a set of experimental data and are strongly case-dependent [33]. In general cases, the validity of models for turbulent characteristics of a spray is questionable. In this study, we propose another methodology to provide input parameters for large-scale turbulence modelling Velikorodny et al. (2015). This methodology does not aim to develop a novel RANS model, but aims to use a different closure. The objective is to assess the performance of a simple mechanistic model for the estimation of turbulence characteristics such as turbulent kinetic energy (TKE) k_t as well as the turbulent length scale L_t in a large-scale particle-laden flow.

The current study is organized as follows: Section 2 describes the methodology applied in this study; Section 3 describes briefly the experiments setup DynAsp; Section 4 shows the validation of the numerical simulations using the experimental results of DynAsp; Section 5 discusses the assessment of the mechanistic model of Kenning Kenning (1996) in the DynAsp configuration using the validated numerical results. Conclusions are given in Sect. 6.

2 Methodology

The turbulence parameters resulting from a spray-gas interaction, such as the turbulence intensity u' and the integral length scale L_t, have to be determined as they can be used, for example, (*a*) for characterization of spray efficiency in breaking up of stratified light flammable gases/steam/air atmospheres Malet et al. (2011), or (*b*) can serve as inputs for the flame burning velocity in the large-scale simulations involving flame-spray interactions Velikorodny et al. (2015).

Having a geometry, we can loosely define two zones affected by water spray as shown in Fig. 1. One we shall call, in what follows, the "inertial zone". In this zone, the steady terminal settling velocity is not reached for the majority of the spray droplets. The second zone, further called the "equilibrium zone", where the terminal settling velocity is reached for the majority of the droplets. The geometrical characteristics of the two zones depend on the nozzle characteristics and the geometry of the building where the nozzles are installed. In this paper, a methodology for the estimation of turbulent characteristics in the *equilibrium zone* using simple models is introduced in the following steps:

1. As a first step, we shall validate the two-phase CFD code Neptune Mimouni et al. (2008) using the DynAsp experimental data. The computed flow variables are compared with

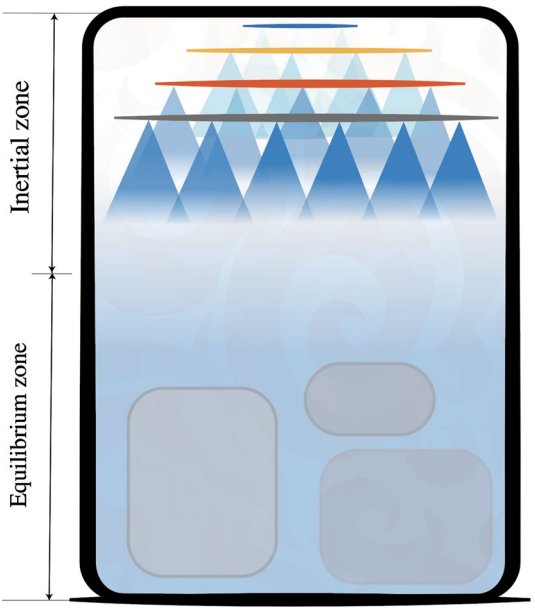

Fig. 1 Industrial spray system containing two regions: inertial zone close to the nozzles and equilibrium zone far from the nozzles

their experimental counterparts. Turbulent characteristics extracted from the computed results are presented and analyzed. Thus validated numerical models can be used later in order to find the turbulence parameters inside the inertial zone.

2. Model of Kenning Kenning (1996) is adapted in order to find the turbulence characteristics inside equilibrium zone of the spray-affected volume. The main input parameter, the slip-velocity, which can be calculated analytically using the Schiller-Naumann drag coefficient correlation Schiller and Naumann (1935).
3. Kenning's model coupled with the slip-velocity correlation is assessed with numerical simulations. The prediction abilities of the simple model on numerical 3D turbulence characteristics are evaluated and discussed.

3 Experimental Setup of DynAsp

A plexiglas box of dimensions of $(0.4 \times 0.4 \times 2.0)\ m^3$ was used in the experiment as depicted in Fig. 2a. A device for injecting glass beads was set on the top of the box. The coordinates system (x, y, z) is defined as shown in Fig. 2b and Fig. 2c, where z is oriented from top to bottom. As shown in Fig. 2a and Fig. 2b, the injection slot has a size of $(88 \times 400)\ mm^2$. The injection has different flow rates of uniform-size particles which are released without initial velocities. Under the effect of gravity, the particles accelerate during the free fall. After the injection, the measurements are performed during 30 seconds after a waiting time of 15 seconds.

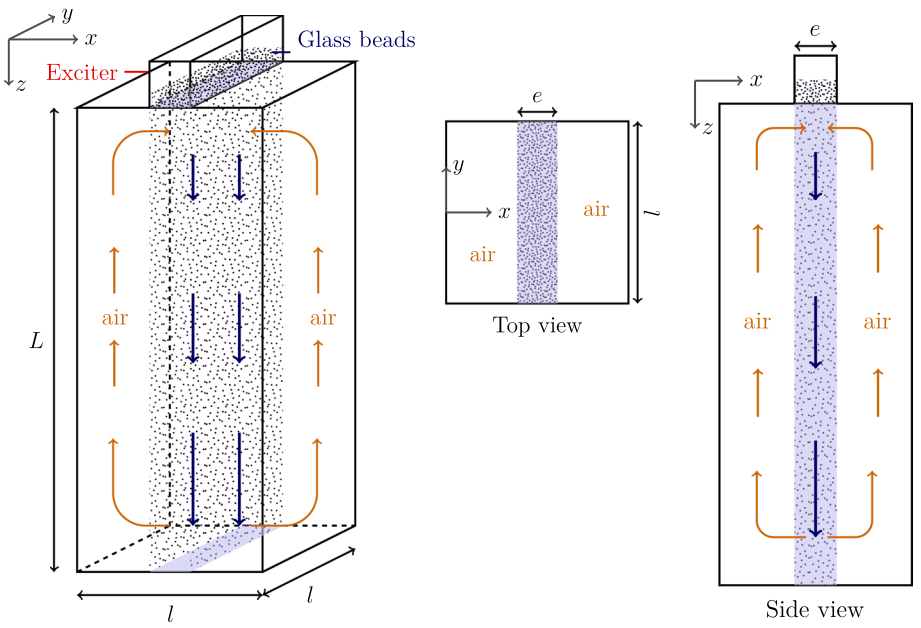

Fig. 2 Dimensions and coordinate system of the experimental setup; **a** main geometry, **b** top view, **c** side view of the setup, with $L = 2\ m$, $l = 0.4\ m$ and $e = 88\ mm$

In this study, we consider particles of diameter, $d_p = 500\ \mu m$. The numerical results are firstly validated against experimental data and then used to assess the predictive behavior of the mechanistic model of Kenning Kenning (1996). Particles characteristics are given in the Table 1.

4 Numerical Modelling

The NEPTUNE_CFD code used in this study, is a three-dimensional multi-fluid Navier-Stokes solver developed jointly by EDF (Électricité de France) and CEA (Commissariat à l'Énergie Atomique et aux Énergies Alternatives) Mimouni et al. (2008),[38]. The solver relies on a finite volume discretization and allows the use of various mesh types (tetra or hexahedral element) for different flow regimes: compressible/incompressible, steady/unsteady, laminar and turbulent.

4.1 Average Field Equations

In various monographs, the derivations and detailed discussions of the conservation equations for two-phase flow are introduced for Eulerian-Eulerian approaches Ishii and Hibiki (2006); Yeoh and Tu (2010). In this section, a brief summary is given on the two-fluid model used in Neptune_CFD, which is based on mass, momentum and energy conservation laws. The mass conservation equation is given as:

$$\frac{\partial}{\partial t}(\alpha_k \overline{\rho}_k) + \nabla \cdot (\alpha_k \overline{\rho}_k \overline{V}_k) = \Gamma_k, \quad k = f, p, \tag{1}$$

where α_k is the volume fraction, $\overline{\rho}_k$ the mass density, $\overline{V}_k$ the local mean velocity of the phase k, Γ_k is the interphase mass transfer rate, the subscripts f and p denote the gas phase and the liquid droplets, respectively.

The momentum balance equation gives:

$$\frac{\partial}{\partial t}(\alpha_k \overline{\rho}_k \overline{V}_k) + \nabla \cdot (\alpha_k \overline{\rho}_k \overline{V}_k^2) = -\alpha_k \nabla \overline{p}_k + M_k + \alpha_k \overline{\rho}_k f_g + \nabla \cdot [\alpha_k (\overline{\tau}_k + \overline{\tau}_k^T)], \quad k = f, p, \tag{2}$$

where $\overline{p}_k$ is the gas pressure for phase k, f_g is the gravity acceleration. In this Eulerian-Eulerian modeling, the gravity of fluid is resolved as well as the particle gravity in the governing equation. The buoyancy force on the particles is neglected compared to the particle gravity. $\overline{\tau}_k$, $\overline{\tau}_k^T$ denote the viscous and Reynolds stress tensors, respectively and M_k is the interphase momentum transfer term Pironneau and Mohammadi (1994) containing four components: drag force, lift force, added mass term and turbulent dispersion force. For heavy particles, with respect to gas density $\rho_p \gg \rho_f$, the momentum transfer term reduces to the drag force contribution:

Table 1 Characteristics of the spray particles

$d_p\ (\mu m)$	$\rho_p\ (kg/m^3)$	Mass flow rate (g/s)	Measurement time (s)
200, 500	2450–2550	16–60	30

$$M_f^D = -M_p^D = -\alpha_p \rho_f \frac{3}{4} \frac{C_D}{d_p} ||\overline{v}_p - \overline{u}_f|| (\overline{v}_p - \overline{u}_f). \tag{3}$$

The momentum transfert term M_p^D comes from the definition of the drag force F_d and C_D is the drag coefficient depending on the particle Reynolds number Re_p. These two quantities are discussed in various studies Gai et al. (2020); Mimouni et al. (2008), one can have generally:

$$F_d = \frac{\pi d_p^3}{6\alpha_p} M_p^D \;\; ; \;\; C_D = \frac{24}{Re_p}\left(1 + 0.15 Re_p^{0.687}\right). \tag{4}$$

4.2 Gas and Dispersed Phase Turbulence

4.2.1 Gas Turbulence Model

The second-order $R_{ij} - \varepsilon$ model is used for the description of the gas phase turbulence Speziale et al. (1991). For each component of the Reynolds stress tensor $R_{f,ij}$, one solves:

$$\begin{aligned} \alpha_f \rho_f \frac{D_f \langle u'_{f,i} u'_{f,j} \rangle_f}{Dt} = & \underbrace{-\frac{\partial}{\partial x_k}\left(\alpha_f \rho_f \langle u'_{f,i} u'_{f,j} u'_{f,k} \rangle_f\right)}_{\text{transport}} \\ & \underbrace{-\alpha_f \rho_f \langle u'_{f,i} u'_{f,k} \rangle_f \frac{\partial \overline{u}_{f,j}}{\partial x_k} - \alpha_f \rho_f \langle u'_{f,j} u'_{f,k} \rangle_f \frac{\partial \overline{u}_{f,i}}{\partial x_k}}_{\text{production}} \\ & \underbrace{+\alpha_f \rho_f \left(\langle u'_{f,j} u'_{f,k} \rangle_f G_{f,ik} + \langle u'_{f,k} u'_{f,i} \rangle_f G_{f,jk}\right) + \alpha_f \rho_f C_0 \varepsilon_f \delta_{ij}}_{\text{drift}} \\ & + \underbrace{\alpha_f \rho_f \langle A_{p \to f,i} u'_{f,j} + A_{p \to f,j} u'_{f,i} \rangle_f}_{\text{interphase exchange}}. \end{aligned} \tag{5}$$

where $\frac{D_f}{Dt} = \frac{\partial}{\partial t} + \overline{u}_{f,j} \frac{\partial}{\partial x_j}$, $\langle \cdot \rangle_f$ operator stands for the mass statistic average; On the right-hand-side of the equation, we have the transport and production terms of Reynolds stress. The pressure fluctuation terms are neglected in this modeling, since the gas flow is considered to be incompressible. The drift term is a closure to the sum of the pressure-deformation correlation term $\Phi_{f,ij}$ and the dissipation term $-\frac{2}{3}\varepsilon_f \delta_{ij}$, which satisfies:

$$\langle u'_{f,j} u'_{f,k} \rangle_f G_{f,ik} + \langle u'_{f,k} u'_{f,i} \rangle_f G_{f,jk} + C_0 \varepsilon_f \delta_{ij} = \Phi_{f,ij} - \frac{2}{3} \varepsilon_f \delta_{ij}. \tag{6}$$

where $C_0 = 2.1$ is the constant of Kolmogorov, and the drift coefficient $G_{f,ij}$ is supposed to be isotropic with an expression:

$$G_{f,ij} = -\frac{1}{\tau_f} \delta_{ij} = -\left(\frac{1}{2} + \frac{3C_0}{4}\right) \frac{\varepsilon_f}{k_t} \delta_{ij} \tag{7}$$

with τ_f the Lagrangian time integral scale of the fluid. The interphase coupling term $\langle A_{p\to f,i}u'_{f,j} + A_{p\to f,j}u'_{f,i}\rangle_f$ represents the Reynolds stress exchange due to the presence of particles or droplets in the fluid, defined as Neiss (2006):

$$\begin{aligned}\langle A_{p\to f,i}u'_{f,j} + A_{p\to f,j}u'_{f,i}\rangle_f = -\chi\frac{1}{\tau_p}[\overline{V}_{d,j}(\overline{u}_{f,i}-\overline{v}_{p,i}) + \langle u'_{f,i}u'_{f,j}\rangle_f - \langle v'_{p,i}u'_{f,j}\rangle_p \\ + \overline{V}_{d,i}(\overline{u}_{f,j}-\overline{v}_{p,j}) + \langle u'_{f,j}u'_{f,i}\rangle_f - \langle v'_{p,j}u'_{f,i}\rangle_p],\end{aligned} \tag{8}$$

where $\chi = \frac{\alpha_p\rho_p}{\alpha_f\rho_f}$ and $\overline{V}_d$ denotes the drift velocity. The drag acceleration term $A_{p\to f,i}$ describes the inverse coupling of the particle on the fluid, of which the average can be expressed as Minier and Peirano (2001):

$$\langle A_{p\to f,i}\rangle_f = \langle -\chi\frac{v_{s,i}-v_{p,i}}{\tau_p}\rangle_f = -\frac{\chi}{\tau_p}(\overline{u}_{f,i} + \overline{V}_{d,i} - \overline{v}_{p,i}), \tag{9}$$

where $v_{s,i}$ is the velocity of fluid seen par the particles Simonin (1991) and τ_p is the particle characteristic response time. It needs to be clarified that the drag acceleration term $A_{p\to f,i}$ is used to characterize the two-phase coupling in the turbulence model. It is different from the momentum transfer term M_p^D in the former section, which is an important term in the average field momentum conservation law. A rigorous treatment of the inverse coupling would imply a multi-point (or multi-particle) probability density function description of the dispersed phase, a choice which was not retained because it is outside the scope of this study.

The advection/diffusion equation for the dissipation rate ε in the $R_{ij}-\varepsilon$ model is:

$$\begin{aligned}\alpha_f\rho_f\frac{D_f\varepsilon_f}{Dt} = &\underbrace{\frac{\partial}{\partial x_i}\left(\alpha_f\rho_f C_\varepsilon\frac{k_t}{\varepsilon_f}\langle u'_{f,i}u'_{f,j}\rangle_f\frac{\partial\varepsilon_f}{\partial x_j}\right)}_{\text{diffusion}} \\ &\underbrace{-\frac{\varepsilon_f}{k_t}C_{\varepsilon_1}\alpha_f\rho_f\langle u'_{f,i}u'_{f,k}\rangle_f\frac{\partial\overline{u}_{f,i}}{\partial x_k}}_{\text{production}} \underbrace{-C_{\varepsilon_2}\alpha_f\rho_f\frac{\varepsilon_f^2}{k_t}}_{\text{dissipation}} + \underbrace{C_{\varepsilon_3}\frac{\varepsilon_f}{k_t}\langle A_{p\to f,i}u'_{f,i}\rangle_f}_{\text{interphase coupling}}\end{aligned} \tag{10}$$

where $C_\varepsilon = 0.18$, $C_{\varepsilon_1} = 1.44$, $C_{\varepsilon_2} = 1.92$ and $C_{\varepsilon_3} = 1.2$ are model constants, and the coupling term $\langle A_{p\to f,i}u'_{f,i}\rangle_f$ can be defined as Oesterlé (2006):

$$\langle A_{p\to f,i}u'_{f,i}\rangle_f = -\chi\frac{1}{\tau_p}[\overline{V}_{d,i}(\overline{u}_{f,i}-\overline{v}_{p,i}) + 2k_t^2 - q_{fp}]. \tag{11}$$

where k_t is the turbulent kinetic energy, q_{fp} is the fluid-particle covariance. The expression of this coupling term can be deduced using Eq. (9).

4.2.2 Dispersed Phase Turbulence Model

The dispersed phase turbulence model used in this study is the $R_2 - Q_{12}$ model Simonin (1991), which contains of the transport equations of the particle Reynolds stress tensor $R_{p,ij}$ and the fluid-particle covariance q_{fp}. The particle stress equation is written as:

$$\alpha_p\rho_p\frac{D_p\left\langle v'_{p,i}v'_{p,j}\right\rangle_p}{Dt} = \underbrace{-\frac{\partial}{\partial x_k}\left(\alpha_p\rho_p\langle v'_{p,i}v'_{p,j}v'_{p,k}\rangle_p\right)}_{\text{transport}} \underbrace{-\alpha_p\rho_p\frac{2}{\tau_p}\left[\langle v'_{p,i}v'_{p,j}\rangle_p - R_{fp,ij}\right]}_{\text{interphase coupling}} \underbrace{-\alpha_p\rho_p\langle v'_{p,i}v'_{p,k}\rangle_p\frac{\partial\overline{v}_{p,j}}{\partial x_k} - \alpha_p\rho_p\langle v'_{p,j}v'_{p,k}\rangle_p\frac{\partial\overline{v}_{p,i}}{\partial x_k}}_{\text{production}}, \tag{12}$$

where $\frac{D_p}{Dt} = \frac{\partial}{\partial t} + \overline{v}_{p,j}\frac{\partial}{\partial x_j}$. The first term on the right is the transport of the particle Reynolds stress tensor. The last two terms are production terms containing velocity gradients. In the interaction coupling term, $R_{fp,ij}$ is the symmetrical part of the correlation tensor between the velocities of the fluid and particles:

$$R_{fp,ij} = \frac{1}{2}\left[\langle v'_{p,j}u'_{f,i}\rangle_p + \langle v'_{p,i}u'_{f,j}\rangle_p\right]. \tag{13}$$

The fluid-particle covariance equation can be written as:

$$\alpha_p\rho_p\frac{D_p(q_{fp})}{Dt} = \underbrace{-\frac{\partial}{\partial x_k}\left(\alpha_p\rho_p\langle u'_{f,i}v'_{p,i}v'_{p,k}\rangle_p\right)}_{\text{transport}} + \Omega_{fp} \underbrace{-\alpha_p\rho_p\frac{q_{fp}}{\tau_f}}_{\text{destruction}} \underbrace{-\alpha_p\rho_p\langle u'_{f,i}v'_{p,k}\rangle_p\frac{\partial\overline{v}_{p,i}}{\partial x_k} - \alpha_p\rho_p\langle v'_{p,i}v'_{p,k}\rangle_p\left(\frac{\partial\overline{u}_{f,i}}{\partial x_k} + \frac{\partial\overline{V}_{d,i}}{\partial x_k}\right)}_{\text{production}} \tag{14}$$

On the right hand side of Eq. (14) one can find the terms of transport, interphase coupling, production and a destruction term for the fluid-particle covariance. The $\langle\cdot\rangle_p$ operator stands for the mass statistic average, τ_f is the time scale of the gas phase movement, Ω_{fp} denotes the coupling between two phases:

$$\Omega_{fp} = \chi\frac{\alpha_p\rho_p}{\tau_p}(q_{fp} - 2q_p^2) + \frac{\alpha_p\rho_p}{\tau_p}(2k_t - q_{fp}). \tag{15}$$

The first term in Ω_{fp} is related to the particle turbulent kinetic energy and the second term is dependent on the fluid turbulent kinetic energy. The term $\frac{\alpha_p\rho_p}{\tau_p}q_{fp}$ represents a source of energy due to the coupling of the fluctuating movement of the two phases. Inversely proportional to τ_p, this term becomes strong as the drops are small, which is consistent with the fact that the smaller the drops, the more sensitive they are to the turbulent fluctuations of the surrounding gas.

The variation of the fluid turbulent kinetic energy k_t with the presence of particles can be expressed as:

$$\alpha_f \rho_f \frac{D_f k_t}{Dt} = \underbrace{-\frac{1}{2}\frac{\partial}{\partial x_k}\left(\alpha_f \rho_f \langle u'_{f,i} u'_{f,i} u'_{f,k} \rangle_f\right)}_{\text{transport}} - \underbrace{\alpha_f \rho_f \varepsilon_f}_{\text{dissipation}}$$
$$\underbrace{-\alpha_f \rho_f \langle u'_{f,i} u'_{f,k} \rangle_f \frac{\partial \overline{u}_{f,i}}{\partial x_k}}_{\text{production}} + \underbrace{\frac{\alpha_p \rho_p}{\tau_p}(-2k_t + q_{fp})}_{\text{interphase coupling}} + \underbrace{\frac{\alpha_p \rho_p}{\tau_p}[\overline{V}_{d,i}(\overline{v}_{p,i} - \overline{u}_{f,i})]}_{\text{drift}} \tag{16}$$

It is important to know the reverse coupling of the fluid turbulent kinetic energy k_t since it is required in several coupling terms mentioned above, such as Eqs. (7), (11) and (15), etc. The drift term represents the modification of the turbulent kinetic energy of the gas due to the transport of the drops by the fluid turbulence. This term can be positive or negative depending on the relative velocity between the two phases.

More details about the model validation and the different interphase coupling terms, such as Eqs. (8), (11) and (15), can be found in Neiss (2006); Simonin (1991); Mimouni et al. (2008); Mimouni (2006).

4.3 Geometry and Mesh

The geometry used in this study is shown in Fig. 2a. The mesh is generated using the SALOME platform Ribes and Caremoli (2007). Two different meshes are used with an averaged cell size $\Delta l_1 = 1\ cm$ and $\Delta l_2 = 0.5\ cm$. Figure 3 shows the axial gas and droplet velocity evolution for the two considered meshes. We can see that the change of the mesh size has a relatively small effect, especially on the droplet velocity evolution. The numerical solution can therefore be considered to be mesh-independent.

The bottom boundary condition is an outlet for the solid particles and a wall condition for the gas phase. The accumulation of the particles on the bottom is considered to have little influence on the gas velocities. All boundaries are considered as no-slip for the gas. The

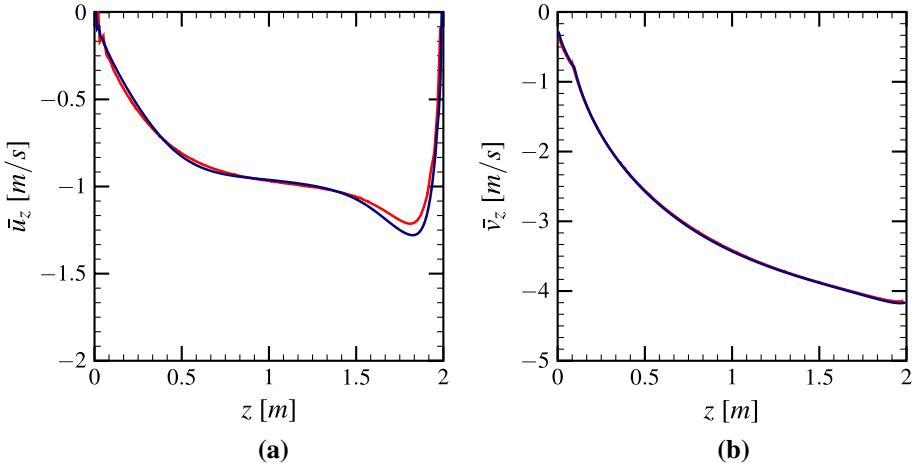

Fig. 3 Spacial distribution of gas and droplet velocities for two different mesh sizes: Δl_1 = 1cm (——), Δl_2 = 0.5cm (——); **a** axial air velocity, **b** axial droplet velocity

collisions between particles as well as the particle-wall interactions are neglected in the current study. The particle-wall interactions are assumed to have small effects on the gas/droplet velocities on the central axis. The walls are considered as adiabatic, with no heat exchange with the fluid.

4.4 RANS Turbulence Modelling for Gas and Particles

A number of comparative numerical studies are performed using the configuration of the experiment DynAsp with different turbulent models. Initial small values for turbulent kinetic energy $k_{t,0} = 10^{-4}\ m^2 s^{-2}$ and dissipation rate $\varepsilon_f = 10^{-3}\ m^2 s^{-3}$ are used. And the turbulence is naturally generated by the coupling between particles and fluids. The injection rate of the particles of $d_p = 500\ \mu m$ is taken as 35 g/s. The numerical results are systematically compared with the experimental measurements. For the measurement of the gas velocity, 10^5 trace particles were taken into account for the calculation of vertical component, and 5×10^4 particles for the horizontal component Patigniez (1996); Herlin et al. (1996). The tracer particle distribution has a Gaussian shape. The program selects the velocity of most counted tracers which is located in the center of the velocity distribution. This velocity is defined as the instantaneous gas velocity. The mean gas velocity is obtained by superposition of several measurements. The experimental standard deviations which represents the validity interval of the measurement are given through error bars (see Fig. 3a).

Figure 4a shows the gas velocity field on the central x-z section for an injection rate of 35 g/s. Two symmetric convective loops can be observed: the gas moves downwards in the central biphasic region and rises up at the pure gas zone. The distributions of the turbulent kinetic energy (TKE) and turbulent dissipation are depicted in Figs. 4b and

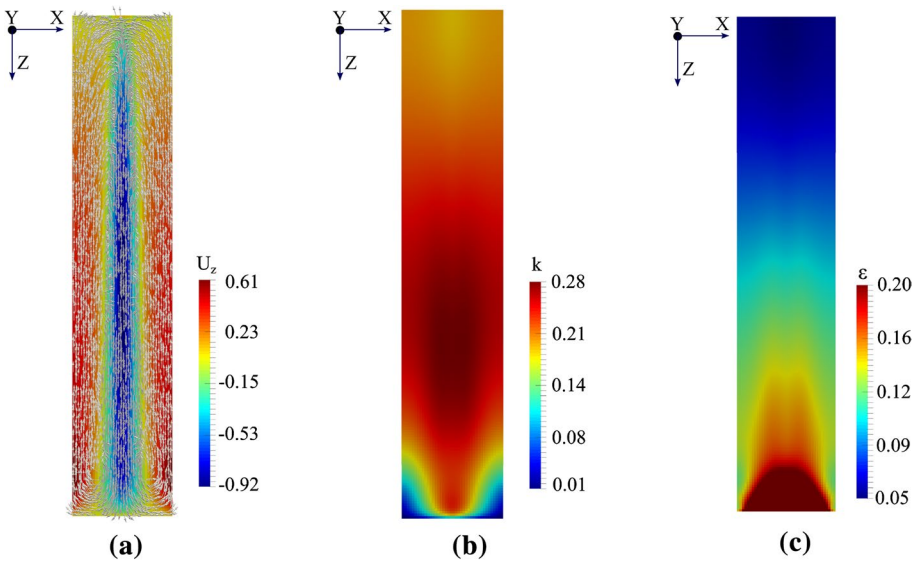

Fig. 4 Numerical simulation showing mean flow quantities: **a** gas velocity (m/s), **b** turbulent kinetic energy (m^2/s^2), **c** turbulent dissipation (m^2/s^3)

4c. It can be seen that the TKE has a maximal value at the lower middle of the biphasic region while the region of high turbulent dissipation rate is located at the bottom of the box. In fact, at the lower middle part of the particle-laden region, the particle velocity gradient becomes small and the production and dissipation of the TKE have very close values.

4.5 Numerical Validation with Reynolds Stress Model

Figure 5a shows the axial velocity of air on the centerline of the box as a function of distance from the injection slot, for two different loading rates: 16 *g/s* and 60 *g/s*. The simulation results of Neptune_CFD are compared to the corresponding experimental data. For all mass injection rates, the particles accelerate along the vertical direction, which through drag forces create the air motion. The larger the mass injection rate is, the faster the axial air velocity becomes. The gas velocity reduces to a small value at the bottom of the domain.

The behavior of the particle velocity as a function of distance from injection slot is given in Fig. 5b. The particles accelerate along the vertical direction. We can see that the height of the experimental set-up is not sufficient for the particles to reach a terminal velocity. The experiments show that the particle velocity evolution is not significantly affected by the change of the mass injection rate. However, the numerical simulation highlights the effects of different mass injection rate. Intuitively, the more particles appear in the flows, the easier the air accelerates.

Generally, we have a good agreement between the numerical and experimental results. The $R_{ij} - \epsilon$ model shows a good performance for the validation of the DynAsp experiments, especially for the predictions of the axial velocities of the air inside the particle/air two-phase flow.

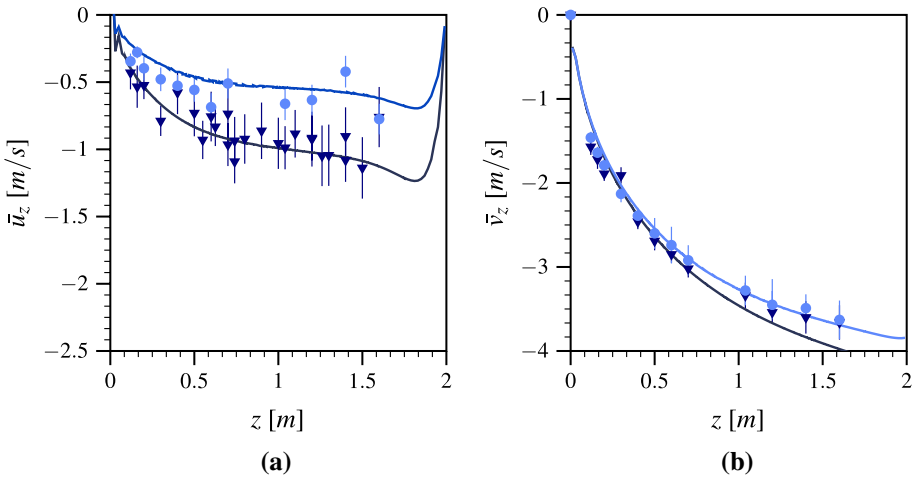

Fig. 5 Comparison of the axial velocity of gas **a** and particles **b** of diameter 500 μm on the centerline for different loading rates: DynAsp 60 g/s (▼), 16 g/s (▾)and (●) Model 60 g/s (——), 16 g/s (——)

4.6 Axial Gas Velocity Near the Wall

The axial gas velocity at the centerline is shown in Fig. 6, with four different injection mass rates: 23 g/s, 35 g/s, 41 g/s and 60 g/s and compared to the experimental data. The error bars and the particle-laden flow borders are also added.

We can see that the numerical estimations of the axial gas velocity confirm the experimental trends for all test cases. Some experimental observations can be confirmed by the numerical simulation, such as the gas velocity increases when approaching the wall. The vertical gas velocity is negative inside the particle flow, and turns to positive near the wall. It can be noted that the gas velocities at two vertical position $z = 0.74\ m$ and $z = 1.26\ m$ have slight difference. And the numerical results match well the experimental measurements inside the two-phase region.

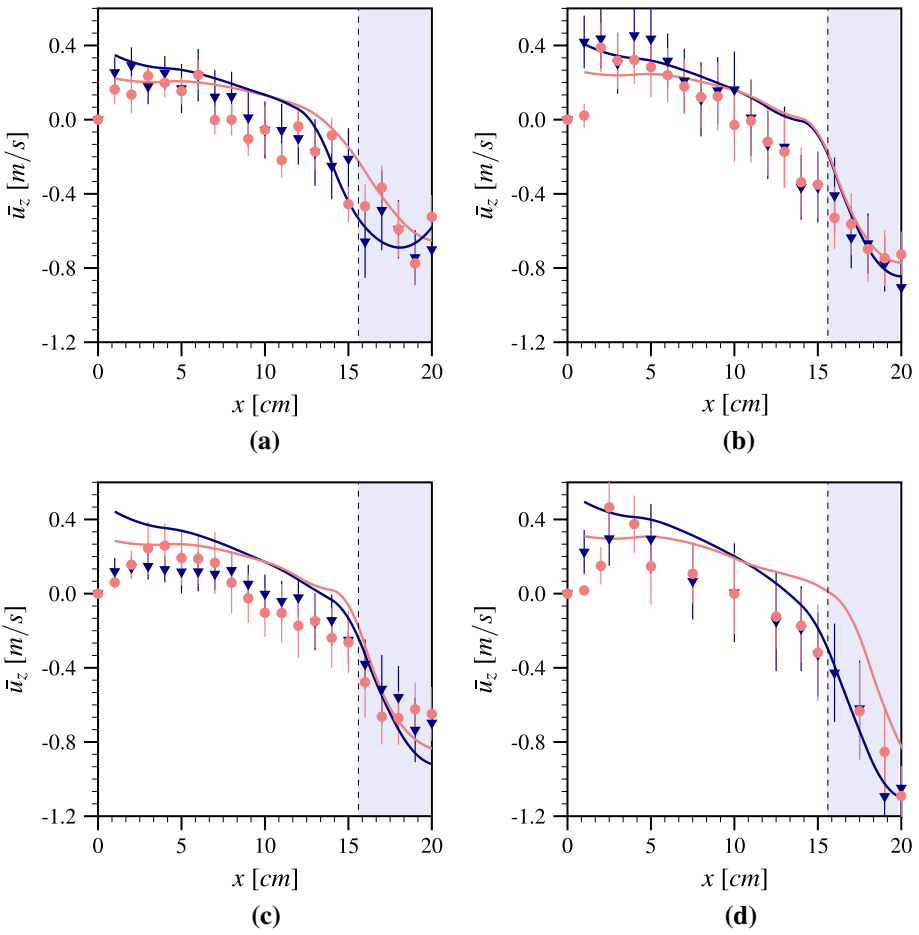

Fig. 6 Axial gas velocity distribution as a function of wall distance; experimental results at $z = 0.74\ m$(▾), $z = 1.26\ m$ (●)and numerical results at $z = 0.74\ m$ (——), $z = 1.26\ m$ (——); particle cloud border (- - -); injection rate **a** 23 g/s, **b** 35 g/s , **c** 41 g/s, **d** 60 g/s. Note that the wall is located at $x = 0$

5 Comparison between Numerical Simulations and the Kenning Model Kenning (1996)

The turbulence modulation by falling solid beads were investigated by Kenning (1996) using a one-dimensional energy balance for validation of experimental data. A mechanistic model was proposed for the estimation of the length scale of the particle-induced turbulence. Initially, the particles are introduced into a still fluid, when the particles reach their *terminal velocity*, the motion of the particle cloud is considered to be the only source of turbulence. The loss of energy of the carrier phase can be divided into two parts: viscous dissipation and particle velocities fluctuations. When the subsequent particles encounter the carrier phase with fluctuating components, the turbulent energy can be redistributed to the particles (see A for more details).

5.1 Mechanistic Model Compared to Numerical Simulations

Five axial probes are used to measure the flow velocities inside the two-phase flow domain. The probe locations are shown in Fig. 7a. The evolution of different parameters such as gas/droplet velocity, integral length scale and kinetic turbulence energy are estimated RANS numerical simulations.

The mechanistic model of Kenning needs to have three input parameters: gas velocity u_f, particle velocity v_p and particle volume fraction α_p, to estimate the kinetic turbulence energy k_t and the integral length scale L_t (see A for more details). These parameters are space and time dependent. Figure 7 shows the variation of these three parameters along the z axis at 5 probe positions.

From Fig. 7c we can see that the volume fraction of the droplets decreases with the vertical distance and reaches a stable value of $\mathcal{O}(10^{-4})$ at the bottom of the geometry. Figs. 7b and 7d show the evolution of the axial gas velocity and the axial slip-velocity. We can see that the probes 1 and 3 give the same values for gas and slip-velocity since they are symmetric relative to the center (the same case for probe 2 and 4).

Given the values of $\bar{u}_z$, $\bar{v}_z$ and α_p at the centerline probe as input parameters, we can use the Kenning model to predict the kinetic turbulence energy and the integral length scale as depicted in Fig. 8. The calculation results of Neptune_CFD are also given for comparison. The turbulent kinetic energy k_t extracted directly from the numerical results and the integral length scale L_t is given by the expression: $L_t = C_\mu^{3/4} k_t/\varepsilon$, where $C_\mu \approx 0.09$ is a constant.

Figure 8 gives the comparison between the numerical simulations and the mechanistic model in the centerline of the lower-part of the DynAsp experimental setup. It is assumed that in this region, the turbulence is homogeneous and isotropic. From Fig. 8a, we can see that the mechanistic model using the input parameters of the central probe can give a good tendency for the kinetic turbulence energy. The values of k_t for different vertical distances have the same order of magnitude as Neptune_CFD. Generally, the mechanistic model can be used to estimate the turbulence intensity if the input values for the volume fraction α_p, gas velocity u_f and especially the slip-velocity $v_p - u_f$ are well estimated.

Similar results can be obtained for the integral length scale. The mechanistic model can provide a prediction of L_t of correct order of magnitude (see Fig. 8b). The difference of the model estimation and the numerical simulations can be due to the geometrical configurations used in the DynAsp experiments. From Fig. 2a, we can see that particles are injected

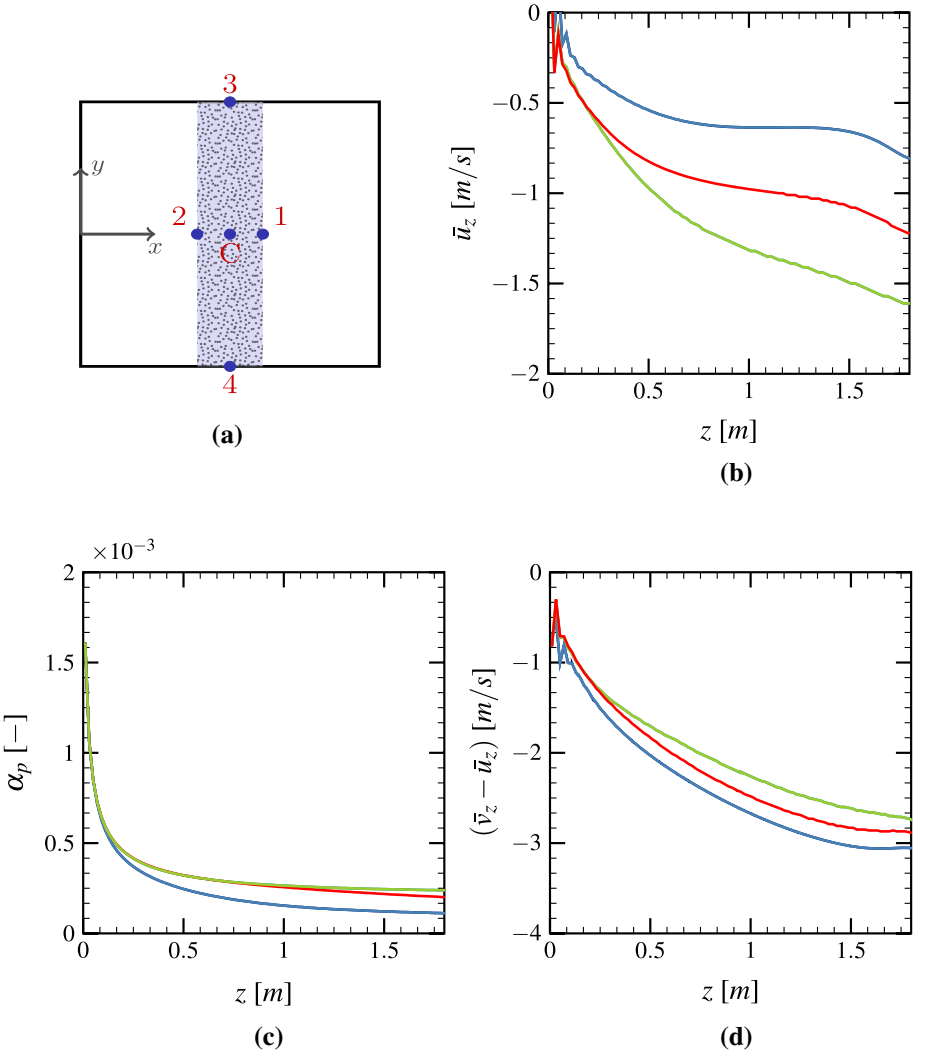

Fig. 7 Numerical results of Neptune_CFD code. **a** Positions of the axial probes. Spatial evolutions of physical properties, **b** axial gas velocity, **c** volume fraction, **d** slip-velocity, for different probes: probe 1 (——), probe 2 (——), probe 3 (——), probe 4 (——)-, center (——). The numerical results for probes 1, 2 and 3, 4 are fully super-imposed due to symmetry

in a small section in the middle of the experimental domain. However, the mechanistic model has been validated for homogeneous particle-laden flows Kenning (1996). Given a larger inter-particle distance λ, the difference between the numerical results and model estimations can be reduced. For example, the model predictions with 1.1λ, 1.2λ or 1.3λ are given in Fig.8b.

The mean volume fraction of the droplets α_p can be referred to the industrial measurements under the particle injection system. In the study of Kenning (1996), u_f is the terminal velocity of the free-fall particles, which plays a minor role on the determination of the

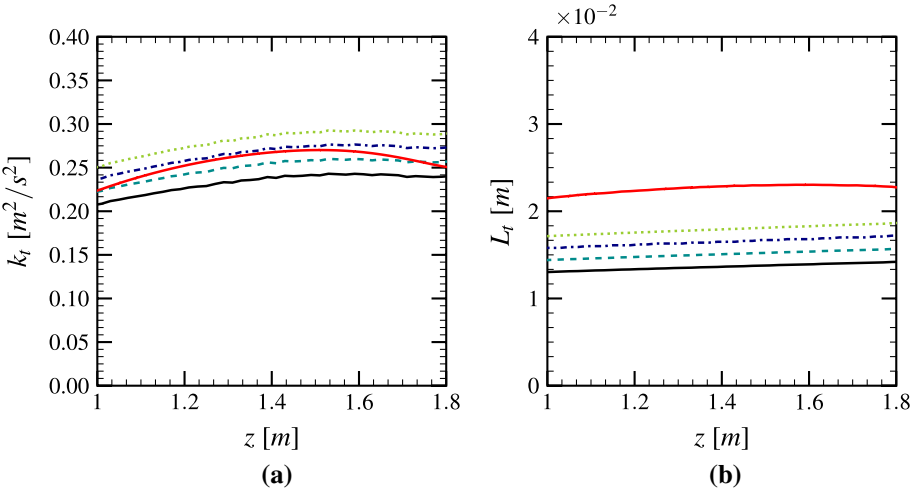

Fig. 8 Kenning's model prediction (——) v.s. numerical results of Neptune_CFD in the centerline (——); the mechanistic model with 1.1λ as inter-particle distance (- - -), with 1.2λ (-·-·-), with 1.3λ (·····); **a** turbulent kinetic energy, **b** integral length scale

kinetic turbulence energy. Thus, the most important parameter to be determined is the slip-velocity $\bar{v}_p - \bar{u}_f$. For the configuration of DynAsp, where the initial velocities of the particles are zero, the terminal slip-velocity can be easily estimated by correlations as discussed in Sect. 5.3.

5.2 Turbulent Length-scale

It was shown that the turbulence enhancement is mainly driven by the dynamics of large droplets Wingerden and Wilkins (1995). For instance, in water spray system, the large-scale turbulence generated from the *bulk* flow of water from the nozzles is considered to be the reason for the flame speed increase. To support this idea, Wingerden *et al.* Wingerden and Wilkins (1995) designed an experiment involving spray and premixed flame in interaction, and used the formula proposed by Hinze (1987), for the estimation of turbulence parameters of the gas mixture affected by a spray:

$$\Lambda_f = (2\pi\nu t_d)^{1/2} \tag{17}$$

where Λ_f is the Eulerian integral length scale of turbulence, ν is the kinematic viscosity, and t_d is the time for turbulence decay. The tests in Wingerden and Wilkins (1995) show that the turbulence exists in the mixture affecting the flame propagation up to 10 s after switching off the spray system. This decay time indicates that the length scale of the spray-generated-turbulence would be of the order of $\Lambda_{spray} = 3\ cm$.

According to the experimental data given in Wingerden and Wilkins (1995), we take, for example, the case of spray with average droplet size of 500 μm, with flow rate of 99 l/min. The kinetic viscosity is taken $\nu = 1.43 \times 10^{-5}\ m^2/s$. Since the volume fraction of spray droplets was not given in Wingerden and Wilkins (1995), we assume that $\alpha_p = 1 \times 10^{-4}$. We can therefore calculate the inter-particle spacing $\lambda = 0.00818\ m$. Taking the width of the experimental box as the integral dissipation length scale $L_i = 1\ m$, equation (34) gives

$L_h = 1.62\ cm$, which matches the order of magnitude of $\Lambda_{spray} = 3\ cm$. Both estimations are close to our results as depicted in Fig. 8.

5.3 Terminal Slip-velocity

In a particle-laden flow, the particle terminal velocity in a cloudy bulk flow is related to the particle volume fraction, which can not be determined analytically. However, the slip-velocity is independent of the injection rate when the particle reaches its terminal velocity. Basing on the force balance, the terminal particle slip-velocity can be calculated by:

$$u_s = \sqrt{\frac{4}{3}\frac{(\rho_p - \rho_f)\ d_p\ f_g}{\rho_f\ C_d}}, \tag{18}$$

where f_g is the gravity acceleration, d_p is the particle diameter, ρ_p and ρ_f denote the particle and gas density, respectively. C_d represents the drag coefficient, which can be calculated using the Schiller-Naumann correlation Schiller and Naumann (1935):

$$C_d = \frac{24}{Re_p}\left(1 + 0.15 Re_p^{0.687}\right) \quad \text{with} \quad Re_p = \frac{\rho_f\, d_p\, u_s}{\mu_f} \tag{19}$$

where Re_p is the particle Reynolds number and μ_f denotes the air viscosity. By combining Eqs. (18) and (19), one can solve a nonlinear equation to obtain the slip-velocity $u_{s,corr}$. The terminal slip-velocity is the relative velocity of the solid particles when the viscous resistance of the carrier phase is equal to the gravity. If the carrier phase is stationary and infinite, the slip-velocity is equal to the particle terminal velocity.

Using similar geometry as the one used in DynAsp tests but having a much larger height $H = 8\ m$, the assessment of this correlation using different particle diameters d_p and particle densities ρ_p is studied. A longer geometry is used to calculate the slip-velocity $u_{s,Nep}$ in Neptune_CFD. The comparison between the results for slip-velocity of Neptune_CFD and the correlation is given in the Table 2. The particles of diameter $d_p = 500\ \mu m$ and density $\rho_p = 2550\ kg/m^3$ are used in all these simulations.

Table 2 Validation of the terminal slip-velocity correlation, injection rate 35 *g/s*

$d_p\ (\mu m)$	$\rho_p\ (kg/m^3)$	$u_{s,Nep}\ (m/s)$	$u_{s,corr}\ (m/s)$	Error %
50	2500	0.21	0.18	14
100	2500	0.54	0.55	1.9
200	2500	1.34	1.41	5.2
300	2500	2.12	2.23	5.2
400	2500	2.86	2.98	4.2
500	2500	3.55	3.69	3.9
50	1000	0.074	0.07	5.4
100	1000	0.25	0.24	4
200	1000	0.70	0.71	1.4
300	1000	1.12	1.17	4.5
400	1000	1.54	1.61	4.5
500	1000	1.95	2.02	3.5

We can see that the equation (18) exhibits a good trend of terminal slip-velocity for particles larger than 50 μm. The relative error is less than 10% for most simulation cales of different droplet diameter and density. Here calculations are done for droplets less than 500 μm with particle Reynolds number equal to $Re_p \approx 1330$. With particles of diameter 100 μm ($Re_p \approx 266$), the correlation (19) can give an estimation having the same order of magnitude as the numerical results.

For smaller particles such as $d_p = 50\ \mu m$, the difference of the slip-velocity estimated can be more important (14% for the case $d_p = 50\ \mu m$ and $\rho_p = 2500\ kg/m^3$). First, the droplets are too small to have a stable terminal slip-velocity while falling down to the bottom of the tube. Moreover, the droplet velocity approaches the air velocity for these small particles. Therefore, the value of the terminal slip-velocity becomes small which leads to large relative errors. As a conclusion, the correlation can be used to estimate the terminal slip-velocity for particles ($d_p 50\ \mu m$). The particles of smaller diameter ($d_p < 50\ \mu m$) have a less important influence on the turbulence generation Crowe et al. (1996); Wingerden and Wilkins (1995). It is noted that the mass flow rate has less influence on the terminal slip-velocity.

Figure 9 shows the slip-velocity evolutions for different initial injection axial velocities at the center of the two-phase flow domain. We can see that the difference of the injection velocity has an influence on the slip-velocity at the first half of the jet. After the stabilization, the slip-velocity decrease/increase to a constant value which is close to the case of spray without initial injection velocity. Thus, if the height of the geometry studied is long enough, the initial velocity effect on the terminal slip-velocity can be neglected for the far field region from injection.

6 Summary

The particle-induced turbulence in a large-scale geometry is investigated numerically by means of 3D RANS calculations and a simple predictive model based on Kenning modelling approach. The obtained results are in good agreements with the experimental data of DynAsp on the particle velocity and air velocity evolutions. The model is compared to the numerical

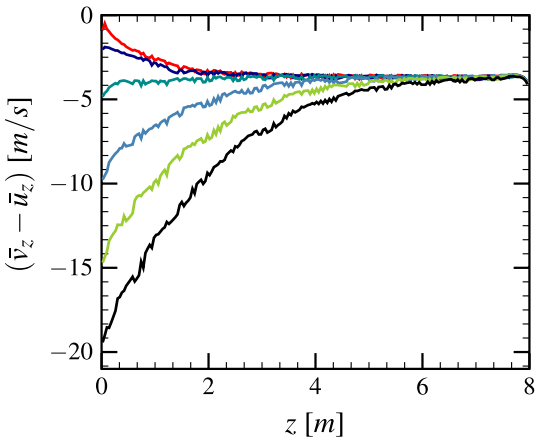

Fig. 9 Slip-velocity as a function of the channel height for different initial velocities v_0; $v_0 = 0\ m/s$ (——), $v_0 = 2\ m/s$ (——), $v_0 = 5\ m/s$ (——), $v_0 = 10\ m/s$ (——), $v_0 = 15\ m/s$ (——), $v_0 = 20\ m/s$ (——)

simulation results and it shows a good capacity to estimate the kinetic turbulence energy and the integral length scale inside the equilibrium zone.

The slip-velocity between the particle and the gas flow is proved to be an important parameter for the estimation of the turbulence intensity. An empirical correlation is compared to the numerical simulations, which can be used to provide the terminal slip-velocity for particles of diameters of the order of $\mathcal{O}(100)\ \mu m$. According to the numerical results, the initial velocity of the injection particles is noted to have very small influence on the terminal particle slip-velocity in the equilibrium zone far from the injection region.

Using the Kenning model and the terminal slip velocity equation, we can estimate the turbulent kinetic energy and the turbulent length scale inside the equilibrium zone generated by falling particles with a sufficient accuracy for large-scale numerical simulations. The simple mechanistic model is proved to be capable of providing reasonable estimations of the turbulent characteristics which can be implemented in large-scale modelling in future studies. This method can be applied to the simulation of slow flame-spray interaction in industrial scenarios such as nuclear containment building, offshore facilities, etc. The future work will consist of estimation of the turbulence parameters inside the *inertial zone*. This will be done through extensive validation of the numerical simulations using available experimental data on the near field of the industrial nozzles.

Appendix

A Mechanistic Model of Kenning et al. Kenning (1996)

For simplicity, the distribution of the dispersed phase is considered as uniform and the fluctuations induced in the carrier phase by the particles are assumed to be isotropic, even though the fluctuation in the streamwise direction is almost twice the fluctuation in the transverse direction Parthasarathy and Faeth (1990).

Since both the carrier flow and the dispersed phase exhibit fluctuating behavior, the relative fluctuations are used to investigate the turbulent energy production and dissipation due to the presence of particles. The relative particle velocity fluctuations were described from the spherical-particle motion equation as:

$$\frac{dv_p'}{dt} = \frac{1}{\tau_p}(u' - v_p') + \frac{1}{2}\frac{\rho_f}{\rho_p}\frac{d(u' - v_p')}{dt}, \tag{20}$$

where ρ_f, ρ_p denote the density of the carrier fluid and the dispersed particle, respectively and u' and v_p' are the fluid and the particle velocity fluctuations respectively, τ_p is the response time of the particle.

Assuming that the fluctuating velocity components of the fluid and the particle velocity behave as:

$$u' = u_0\, e^{i\omega t}, \quad v_p' = u_0\, \mathscr{A} e^{i\omega t + \phi}, \tag{21}$$

where u_0, $\mathscr{A}u_0$ are the amplitudes of the fluid and the particle velocity fluctuations, respectively and ω is the characteristic frequency of the fluid defined as:

$$\omega = \frac{v_{rel}}{\lambda}, \tag{22}$$

where v_{rel} and λ denote the relative velocity between the two phases and the mean inter-particle distance of the dispersed phase, respectively.

By introducing (21) into Equation (20), we can have:

$$\begin{aligned} \mathscr{A}cos\phi - S_t\, sin\phi\, \mathscr{A}\left(1 + \frac{1}{2}\frac{\rho_f}{\rho_p}\right) &= 1, \\ \mathscr{A}sin\phi + S_t\, cos\phi\, \mathscr{A}\left(1 + \frac{1}{2}\frac{\rho_f}{\rho_p}\right) &= S_t\left(\frac{1}{2}\frac{\rho_f}{\rho_p}\right), \end{aligned} \tag{23}$$

where $S_t = \omega\tau_p$ is the Stokes number.

From Equation (23), we can obtain ϕ and $\mathscr{A}$ as:

$$\phi = arctan\left(\frac{-2S_t}{S_t^2\frac{\rho_f}{\rho_p}\left(1 + \frac{1}{2}\frac{\rho_f}{\rho_p}\right) + 2}\right), \tag{24}$$

$$\mathscr{A} = \sqrt{\frac{1 + tan^2\phi}{\left[1 - S_t\, tan\phi\left(1 + \frac{1}{2}\frac{\rho_f}{\rho_p}\right)\right]^2}}, \tag{25}$$

Kenning *et al.* Kenning (1996) propose a simple expression of the fluctuation amplitude $\mathscr{A}$ using the Stokes number, such as:

$$\mathscr{A} = \sqrt{\frac{S_t^2\frac{\rho_f^2}{\rho_p^2} + 4}{4S_t^2 + 4S_t^2\frac{\rho_f}{\rho_p} + S_t^2\frac{\rho_f^2}{\rho_p^2} + 4}}. \tag{26}$$

We can notice from Equation (26) that $\mathscr{A}$ is smaller than unity, which indicates that the particles oscillation magnitude is smaller than that of the fluid fluctuations.

A.1 Turbulence generation by particles

Considering the main flow direction, the kinetic energy transfer rate from particles to fluid per unit particle mass due to the velocity difference can be estimated by:

$$P_p = \frac{(u - v_p)^2}{\tau_p}, \tag{27}$$

where u and v_p are fluid and particle instantaneous velocity, respectively. τ_p is the mean particle response time. The velocities can be divided into mean and fluctuating parts as:

$$\begin{aligned} u &= \overline{u} + u', \\ v_p &= \overline{v}_p + v_p', \end{aligned} \tag{28}$$

Considering the expression of Equation (21), we can calculate the averaged energy production rate as:

$$\overline{P}_{p,1} = \frac{1}{2}\left[\frac{2\,(\overline{u}-\overline{v}_p)^2 + \mathscr{A}^2\,u_0^2 - 2\,u_0^2\,\mathscr{A}cos\phi + u_0^2}{\tau_p}\right], \tag{29}$$

Even though the kinetic energy transfer is mainly due to the velocity in the main flow direction, the fluctuation of the fluid and the particles are basically three-dimensional. Thus, the turbulent energy production from the particle to the fluid should be three-dimensional, leading to a more general formulation of the turbulent production term:

$$\overline{P}_{p} = \frac{1}{2}\left[\frac{2(\overline{u}-\overline{v}_p)^2 + 3\mathscr{A}^2\,u_0^2 - 6\,u_0^2\,\mathscr{A}cos\phi + 3u_0^2}{\tau_p}\right]. \tag{30}$$

A.2 Energy redistributing to particles

Particle fluctuations are mainly due to the fluid flow fluctuations. The presence of dispersed particles dissipates part of the turbulent energy of the carrier phase. The dissipation rate per unit mass of particles is derived from the following particle equation:

$$\varepsilon_p = \frac{d(\frac{1}{2}v'^2_p)}{dt} = \left[\frac{1}{\tau_p}(u'-v'_p) + \frac{1}{2}\frac{\rho_f}{\rho_p}\frac{d(u'-v'_p)}{dt}\right]v'_p, \tag{31}$$

Using Equation (21), a mean dissipation rate over a complete oscillation period results in:

$$\overline{\varepsilon}_p = 3\times u_0^2\,\mathscr{A}\left[\frac{2cos\phi - 2\,\mathscr{A} + S_t\,sin\phi\frac{\rho_f}{\rho_p}}{4\tau_p}\right]. \tag{32}$$

where the factor 3 indicates that the dissipation of the fluctuations account for three dimensional effect, similar to the turbulence generation.

A.3 Viscous flow dissipation

The presence of particles in the carrier phase will not generate only turbulence, but also modify the viscous dissipation rate of the fluid. The rate of turbulent dissipation proposed by Kenning is:

$$\varepsilon = \frac{k_t^{3/2}}{L_h}, \tag{33}$$

where L_h is the hybrid length scale which combines the inherent integral length scale L_i and the mean inter-particle distance of the dispersed particles λ.

$$L_h = \frac{2}{\frac{1}{\lambda}+\frac{1}{L_i}} = \frac{2L_i\lambda}{L_i+\lambda}. \tag{34}$$

The factor 2 comes from the harmonic average of these two length scales.

Combining (30) and (32), the turbulent kinetic energy rate can be expressed as:

$$\frac{dk_t}{dt} = (\overline{P}_p - \overline{\varepsilon}_p)\left(\frac{\alpha_p}{1-\alpha_p}\right)\left(\frac{\rho_p}{\rho_f}\right) + (P_i - \varepsilon). \tag{35}$$

where α_p denotes the volume fraction of the dispersed phase, and P_i is the inherent turbulence in the carrier fluid for no-stagnant initial conditions.

Acknowledgements The authors gratefully acknowledge the financial support from Electricité de France (EDF) within the framework of the Generation II & III reactor research program.

Declarations

Conflict of interest The authors declare that they have no conflict of interest.

References

Balachandar, S., Eaton, J.K.: Turbulent dispersed multiphase flow. Annu. Rev. Fluid Mech. **42**(1), 111–133 (2010)

Crowe, C.T.: On models for turbulence modulation in fluid-particle flows. Int. J. Multiph. Flow **26**(5), 719–727 (2000)

Crowe, C.T., Troutt, T.R., Chung, J.N.: Numerical models for two-phase turbulent flows. Annu. Rev. Fluid Mech. **28**(1), 11–43 (1996)

Crowe, C.T., Schwarzkopf, J.D., Sommerfeld, M., Tsuji, Y.: Multiphase flows with droplets and particles. Taylor and Francis, CRC (2012)9781439840504

Eaton, J.K.: *Turbulence modulation by particles, Multiphase Flow Handbook (ed. C.T. Crowe)*. CRC, Taylor and Francis, (2006). ISBN 9781498701006

Elghobashi, S.: On predicting particle-laden turbulent flows. Appl. Sci. Res. **52**(4), 309–329 (1994)

Elghobashi, S.: DNS of turbulent flows laden with droplets or bubbles. *ArXiv e-prints*, April (2018)

Gai, G., Hadjadj, A., Kudriakov, S., Thomine, O.: Particles-induced turbulence: A critical review of physical concepts, numerical modelings and experimental investigations. Theor. App. Mech. Lett. **10**, 1–7 (2020)

Gai, G., Kudriakov, S., Rogg, B., Hadjadj, A., Studer, E., Thomine, O.: Numerical study on laminar flame velocity of hydrogen-air combustion under water spray effects. Int. J. Hydrog. Energy **44**(31), 17015–17029 (2019)

Gai, G., Thomine, O., Kudriakov, S., Hadjadj, A.: A new formulation of a spray dispersion model for particle/droplet-laden flows subjected to shock waves. J. Fluid Mech. **905**, A24 (2020)

Gai, G., Thomine, O., Hadjadj, A., and Kudriakov, S.: Modeling of particle cloud dispersion in compressible gas flows with shock waves. *Phys. Fluids*, 32:023301, 02 (2020)

Gexcon AS. FLACS code User Manual, (2020). http://www3.gexcon.com/files/manual/flacs/html/index.html

Gore, R.A., Crowe, C.T.: Effect of particle size on modulating turbulent intensity. Int. J. Multiph. Flow **15**(2), 279–285 (1989)

Gore, R.A., Crowe, C.T.: Modulation of turbulence by a dispersed phase. ASME J. Fluids Eng. **113**(2), 304–307 (1991)

Herlin, L., Mallet, G., Coche, J.-C., and Dumas, P.: Présentation de l'expérience DynAsp. *Technical Report*, (1996)

Hetsroni, G.: Particles-turbulence interaction. Int. J. Multiph. Flow **15**(5), 735–746 (1989)

Hetsroni, G., Sokolov, M.: Distribution of mass velocity and intensity of turbulence in a two-phase turbulent jet. ASME J. Appl. Mech. **38**(2), 315–327 (1971)

Hinze, J.O.: Turbulence. McGraw-Hill, McGraw-Hill classic textbook reissue (1987)

Hosokawa, S., and Tomiyama, A.: Influences of relative velocity on turbulent intensity in gas-solid two-phase flow in a vertical pipe. In *Third Int. Conference on Multiphase Flow, ICMF98*, Lyon, France, (1998)

Ishii, M., Hibiki, T.: Thermo-fluid Dynamics of two-phase flow. Springer, Berlin (2006)

Kenning, V.M., Crowe, C.T.: On the effect of particles on carrier phase turbulence in gas-particle flows. Int. J. Multiph. Flow **23**(2), 403–408 (1997)
Kenning, V.M.: *Self-induced turbulence in solid-liquid flow*. PhD thesis, Washington University, USA, (1996)
Kulick, J.D., Fessler, J.R., Eaton, J.K.: Particle response and turbulence modification in fully developed channel flow. J. Fluid Mech. **277**, 109–134 (1994)
Malet, J., Blumenfeld, L., Arndt, S., Babic, M., Bentaib, A., Dabbene, F., Kostka, P., Mimouni, S., Movahed, M., Paci, S., Parduba, Z., Travis, J., and Urbonavicius, E.: Sprays in containment: Final results of the sarnet spray benchmark. *Nucl. Eng. Des.*, 241(6):2162–2171, (2011). (W3MDM) University of Leeds International Symposium: Multi-dimensional Advances for Industrial Process Monitoring
Mallouppas, G., George, W.K., van Wachem, B.G.M.: Dissipation and inter-scale transfer in fully coupled particle and fluid motions in homogeneous isotropic forced turbulence. Int. J. Heat. Fluid Flow **67**, 74–85 (2017)
Mandø, M.: *Turbulence modulation by non-spherical particles.* PhD thesis, Aalborg Universitet, Denmark, (2009)
Mandø, M., Lightstone, M.F., Rosendahl, L., Yin, C., and Sørensen, H.: Turbulence modulation in dilute particle-laden flow. *Int. J. Heat. Fluid Flow*, 30(2):331 – 338, (2009)
Mimouni, S., Boucker, M., Laviéville, J., Guelfi, A., Bestion, D.: Modeling and computation of cavitation and boiling bubbly flows with the NEPTUNE_CFD code. Nucl. Eng. Des. **238**(3), 680–692 (2008)
Mimouni, S., Archambeau, F., Boucker, M., Laviéville, J., and Morel, C.: A second-order turbulence model based on a reynolds stress approach for two-phase flow. Part i: Adiabatic cases. *Science and Technology of Nuclear Installations*, 2009, 06 (2008)
Mimouni, S.: Modeling and cavitation flows : a two-phase flow approach. *La Houille Blanche*, 6, (2006)
Minier, J.-P., Peirano, E.: The pdf approach to turbulent polydispersed two-phase flows. Phys. Rep. **352**(1), 1–214 (2001)
Neiss, C.: *Modélisation et simulation de la dispersion turbulente et du dépôt de gouttes dans un canal horizontal*. PhD thesis, Université de Grenoble, France, (2006)
Neptune_CFD version 4.3.1 Theory Guide, 2019
Oesterlé, B.: *Ecoulements multiphasiques.* Hermes Science, 2006., (2006)
Parthasarathy, R.N., Faeth, G.M.: Turbulence modulation in homogeneous dilute particle-laden flows. J. Fluid Mech. **220**, 485–514 (1990)
Patigniez, A.: Expérience DynAsp - résultats expérimentaux. *Technical Report*, (1996)
Pironneau, O., and Mohammadi, B.: *Analysis of the k-epsilon turbulence model*. Mason, (1994)
Ribes, A., and Caremoli, C.: Salomé platform component model for numerical simulation. In *31st Annual International Computer Software and Applications Conference (COMPSAC 2007)*, volume 2, pages 553–564, July (2007)
Saber, A., Lundström, T., Hellström, J.: Turbulent modulation in particulate flow: A review of critical variables. Engineering **7**, 597–609 (2015)
Sadiki, A., Chrigui, M., Janicka, J., Maneshkarimi, M.R.: Modeling and Simulation of Effects of Turbulence on Vaporization, Mixing and Combustion of Liquid-Fuel Sprays. Flow Turbul Combust **75**(1), 105–130 (2005)
Schiller, L., Naumann, A.: A drag coefficient correlation. Zeitschrift des Vereins Deutscher Ingenieure **75**, 318–320 (1935)
Simonin, O.: Second-moment prediction of dispersed phase turbulence in particle-laden flows. In *8th Symposium on Turbulent Shear Flow*, Germany, (1991)
Speziale, C.G., Sarkar, S., Gatski, T.B.: Modelling the pressure-strain correlation of turbulence: an invariant dynamical systems approach. J. Fluid Mech. **227**, 245–272 (1991)
Tanaka, T., Eaton, J.K.: Sub-Kolmogorov resolution particle image velocimetry measurements of particle-laden forced turbulence. J. Fluid Mech. **643**, 177–206 (2010)
Thomas, G.O.: On the conditions required for explosion mitigation by water sprays. Process. Saf. Environ. **78**(5), 339–354 (2000)
Tsuji, Y., Morikawa, Y., Shiomi, H.: LDV measurements of an air-solid two-phase flow in a vertical pipe. J. Fluid Mech. **139**, 417–434 (1984)
Velikorodny, A., Studer, E., Kudriakov, S., Beccantini, A.: Combustion modeling in large scale volumes using europlexus code. J. Loss Prevent. Proc. **35**, 104–116 (2015)
Wacks, D., Chakraborty, N.: Flame Structure and Propagation in Turbulent Flame-Droplet Interaction: A Direct Numerical Simulation Analysis. Flow Turbul Combust **96**(4), 1053–1081 (2016)
Wingerden, K.V., and Wilkins, B.: The influence of water sprays on gas explosions. Part 2: mitigation. *J. Loss Prevent. Proc.*, 8(2):61–70, (1995)

Wingerden, K.V., and Wilkins, B.: The influence of water sprays on gas explosions. Part 1: water-spray-generated turbulence. *J. Loss Prevent. Proc.*, 8(2):53–59, (1995)

Xu, Y., Subramaniam, S.: Effect of Particle Clusters on Carrier Flow Turbulence: A Direct Numerical Simulation Study. Flow Turbul Combust **85**(3), 735–761 (2010)

Yarin, L.P., Hetsroni, G.: Turbulence intensity in dilute two-phase flows-3 the particles-turbulence interaction in dilute two-phase flow. Int. J. Multiph. Flow **20**(1), 27–44 (1994)

Yeoh, G.H., and Tu, J.: Chapter 2 - governing equations and boundary conditions. In Guan Heng Yeoh and Jiyuan Tu, editors, *Computational Techniques for Multiphase Flows*, pages 21–94. Butterworth-Heinemann, Oxford, (2010)

Yuan, Z., and Michaelides, E.E.: Turbulence modulation in particulate flows. A theoretical approach. *Int. J. Multiph. Flow*, 18(5):779–785, (1992)